Journal of Civil and Hydraulic Engineering
https://www.acadlore.com/journals/JCHE

Influence of Geogrid Reinforcement on Pipeline Failure Mechanisms under Full Pipe Flow: Insights from Transparent Soil Modelling

Yuanyu Duan[1,2], Weiwen Zhang[1], Zhen Xu[1], Lianguo Cheng[3*], Xu Lu[1]

[1] School of Urban Construction and Transportation, Hefei University, 230601 Hefei, China
[2] Anhui Provincial Key Laboratory of Urban Rail Transit Safety and Emergency Management, Hefei University, 230601 Hefei, China
[3] Anhui Wanjiang Expressway Co., Ltd., 230088 Hefei, China

* Correspondence: Lianguo Cheng (27439065@qq.com)

Received: 03-14-2025 **Revised:** 07-09-2025 **Accepted:** 07-20-2025

Citation: Y. Y. Duan, W. W. Zhang, Z. Xu, L. G. Cheng and X. Lu, "Influence of geogrid reinforcement on pipeline failure mechanisms under full pipe flow: Insights from transparent soil modelling," *J. Civ. Hydraul. Eng.*, vol. 3, no. 3, pp. 168–180, 2025. https://doi.org/10.56578/jche030305.

Abstract: The mechanisms governing underground pipeline rupture in erodible soils remain a critical focus in geotechnical engineering, particularly under full pipe flow conditions. In this study, the impact of geogrid reinforcement on the fracture behavior of buried pipelines was systematically investigated using transparent soil modelling techniques, which enabled real-time visualization of subsurface erosion dynamics. Geogrid reinforcement was applied across varying spatial extents to identify the optimal reinforcement zone for mitigating collapse-induced failure. Soil-particle migration and cavity formation were monitored under different hydraulic scenarios, facilitating a detailed characterization of erosion pit evolution and subgrade instability. Test results demonstrated that appropriately positioned geogrid reinforcement significantly delayed the initiation and progression of subsidence, reduced the depth and volume of collapse zones, and enhanced the structural integrity of the surrounding subgrade. Under pressure-free conditions, geogrid installation was found to slow the erosion rate, whereas under full pipe flow, the reinforcement effectively suppressed sudden cavity collapse and curtailed the expansion of erosion-prone areas. These findings highlight the critical role of geogrid placement in maintaining pipeline stability by moderating soil loss and controlling void development. The use of transparent soil provided unique insights into the spatial and temporal characteristics of internal erosion, allowing for a more precise delineation of geogrid influence zones. This research contributes to a deeper understanding of subsurface failure mechanisms in reinforced systems and offers practical guidance for infrastructure resilience against hydraulic-induced ground deformation.

Keywords: Geogrid; Road surface collapse; Full pipe flow; Soil erosion

1 Introduction

In recent years, ground collapse accidents caused by pipeline fracture and damage have occurred frequently, which not only poses a great safety hazard to pedestrians and vehicles, but also causes huge economic losses. Over time, these pipes may become damaged and leak due to aging and changes in surrounding loads. The rupture and leakage of the pipeline will cause water to seep through the cracks, resulting in the erosion of the surrounding soil and the formation of underground cavities. The soil above these cavities loses support, which will lead to structural instability and eventually lead to ground collapse. Such a collapse would disrupt the city's transportation system, with significant social and economic consequences [1].

Geogrid is widely used in the reinforcement of subgrade filling, which can significantly improve the bearing capacity of foundation [2]. At present, there are a large number of studies on the application of geogrid in road engineering, ranging from retaining wall [3], slope to roadbed [4], foundation treatment [5] and so on. For example, Li et al. [6] found that the overall performance of asphalt mixtures was significantly improved after the use of geogrids; Erdag et al. [7] investigated the engineering properties of the steel slag-subgrade-geogrid composite structure and found that the permanent deformation in the electric arc furnace mixture was reduced by 25% by adding geogrid reinforcement. Hassan et al. [8] found that geosynthetics can effectively improve the stiffness, cohesion and shear strength of cohesive soil. Zhang et al. [9] found that the grid reinforcement can stabilize the crack propagation near

the reinforced layer and reduce the influence depth of the soil-air interface and atmospheric changes on the soil. Santos et al. [10] used the large-scale model of a geogrid-reinforced soil wall to evaluate the performance under different simulated rainfall intensities and drying periods. The research shows that geogrid improves the performance of reinforced soil walls with poor drainage. Elshesheny et al. [11] found that the use of a geogrid layer helps to reduce the deformation of the soil surface. Minchala et al. [12] used geosynthetics as a base to stabilize tunnel silt, landslide debris and recycled asphalt pavement, and found that geosynthetics significantly improved the performance of edge materials. Jiang et al. [13] conducted a comprehensive evaluation of the full-scale inverted pavement. The results show that the addition of geogrid to the unbound aggregate base can improve the rutting resistance. Saily and Gratchev [14] added geosynthetics to expansive soil. It was found that the total expansion of the soil can be reduced. Abdi et al. [15] studied soil deformation and particle displacement at the soil-geogrid interface and near the nail using particle image velocimetry (PIV) techniques.

Transparent soil material is a simulation material that simulates the mechanical properties of natural soil with synthetic materials and remains transparent visually. It is mainly composed of transparent skeleton particles and transparent pore liquid with similar or the same refractive index [16]. As a soil substitute, the test results of geotechnical engineering properties are the same as those of natural soil [17]. Transparent soil technology has become an indispensable and powerful tool in the basic research of geotechnical engineering since the concept breakthrough [18] in the mid-1990s. Some scholars have used the transparent soil model to study the stability of the tunnel face [19]. Yu et al. [20] successfully observed the internal structure and flow velocity in uniform granular soil using transparent soil technology. The transparent soil samples created by Sanvitale et al. [21] using refractive image matching can provide the basic perspective of particle size required for the development of comprehensive insights. Xu and Guo [22] and Le et al. [23] studied the vertical bearing characteristics and load transfer mechanism of pile foundation by using transparent soil technology and analyzing the deformation around the pile. Siemens et al. [24] realized high-resolution saturation measurement in unsaturated transparent soil experiments through digital image analysis, providing new insights into near-surface flow processes. In recent progress, Zhang et al. [25] established a model test system for the grouting process and bearing capacity of gravel piles by using transparent soil and particle image velocimetry (PIV). Ads et al. [26] observed the internal deformation process of soil with the help of a transparent soil model; in the latest progress, Liu et al. [27] studied the influence of foundation pit excavation on adjacent existing tunnels by using a transparent soil scale model and particle image velocimetry technology. Other scholars have used 3D printing technology to improve the potential of geogrids [28]. Duan et al. [29] studied the erosion variation law under different hydraulic conditions through transparent soil technology, and found that when the water flow rate is too fast, a large area of erosion will be formed. Jiang et al. [30] established a visual fluidization simulation device using transparent soil instead of natural sand, and studied the three-dimensional visual process of water-oil interaction after pressure pipeline leakage.

The existing research mainly focuses on the variation of soil erosion under different hydraulic conditions, but the erosion mechanism of soil under full pipe flow and the mitigation effect of reinforcement treatment on collapse have not been fully discussed. Based on the fracture test of transparent soil pipeline under different working conditions [29], this paper continues to discuss the comparison between unreinforced and reinforced in the case of full pipe flow. In this paper, the transparent soil test technology is used to study the influence process of subgrade soil erosion caused by pipeline fracture and leakage under the condition of full pipe flow, and the geogrid reinforcement is set up in the appropriate area for analysis and research. The purpose of this paper is to investigate the mechanism of ground collapse caused by groundwater pipeline rupture and to explore methods for mitigating such collapses. The full pipe flow simulates the influence of pipeline rupture on soil erosion under the condition of tap water transportation and rainstorm. Through the reinforcement treatment of underground soil, it prevents the sudden destruction of the ground caused by the sudden rupture of the pipeline under the condition of full pipe flow, which causes harm to vehicles and pedestrians.

2 Experimental Materials and Methods

2.1 Mechanical Properties of Geogrids

Table 1. Mechanical parameters of geogrid

Tensile Strength / (kN/m)		**Strength at a Given Elongation / (kN/m)**	
long direction	cross direction	2% elongation	5% elongation
45	45	19	22

In this transparent soil test, sandy soil was used, with fused quartz sand as the aggregate and a mixture of n-dodecane and food-grade No.15 white oil as the interstitial solution. The geogrid used is a biaxially stretched plastic material with high tensile strength. The specification is TGSG45-45 and the size is 3×3 cm. The geogrid is

cut into a square to facilitate laying inside the soil. The mechanical parameters of the geogrid are shown in Table 1, and the reinforcement samples are shown in Figure 1.

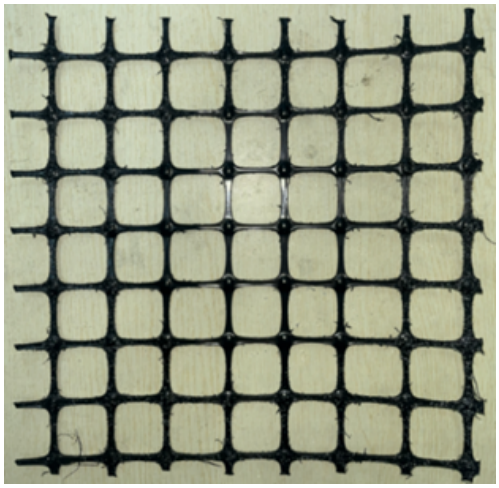

Figure 1. Geogrid sample

2.2 Model Device

In this test, the scale test model is used, the geometric similarity ratio is 30, and the size of the model box is 300*300*300 mm (Figure 2). The scale is scaled according to the size of the actual pipeline in China, and the PVC pipe (outer diameter d is 25 mm) is used to simulate the underground pipeline. The PVC pipe is a standardized pipe diameter, which is convenient for procurement and does not need to be made separately. The whole test device adopts the visual processing of transparent soil technology, which is convenient for analyzing the erosion process and the effect of geogrid reinforcement. In this experiment, the laser source is a 532-1 watt linear optical machine produced by Beijing Bangshou Technology Co., Ltd., and the camera is a Canon EOS 60D SLR camera. The effect of the model sample after the sample is filled is shown in Figure 3.

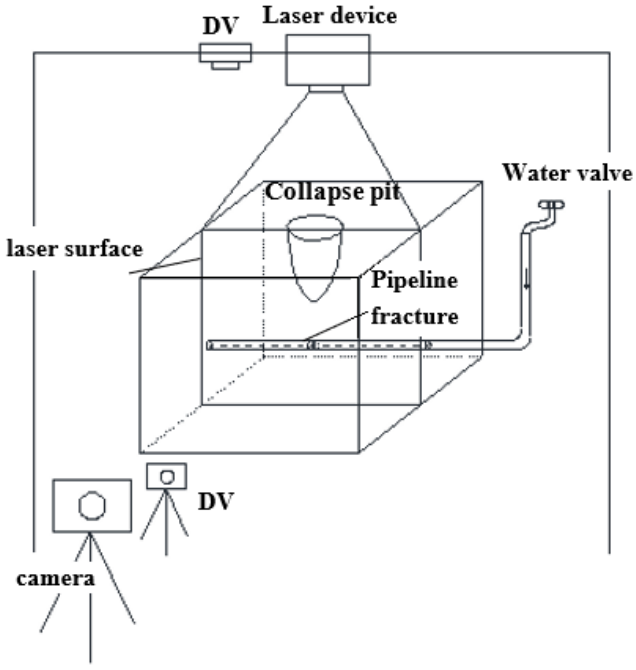

Figure 2. Test device diagram [29]

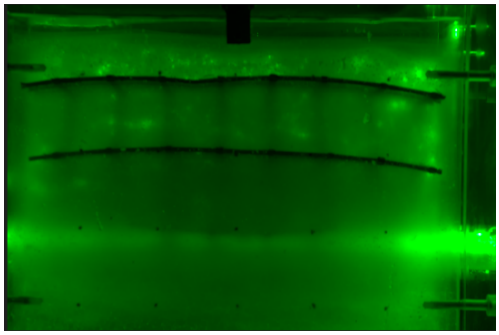

Figure 3. Model sample

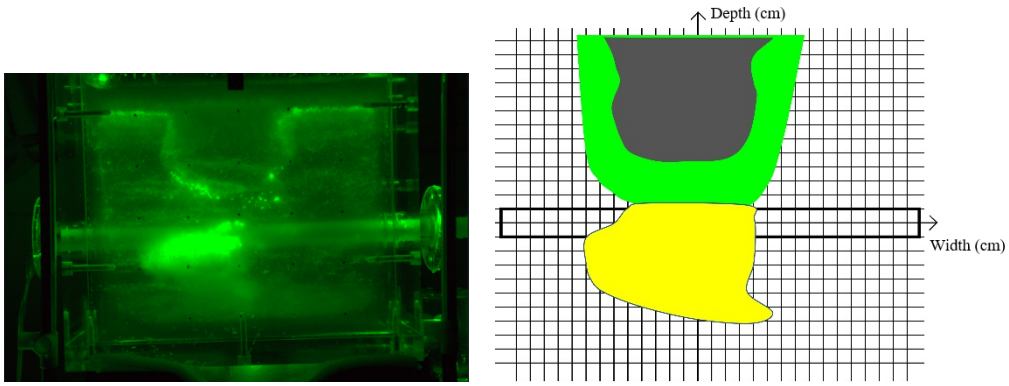

(a) Erosion area distribution (b) Region of particle motion

Figure 4. Unreinforced state of full pipe flow

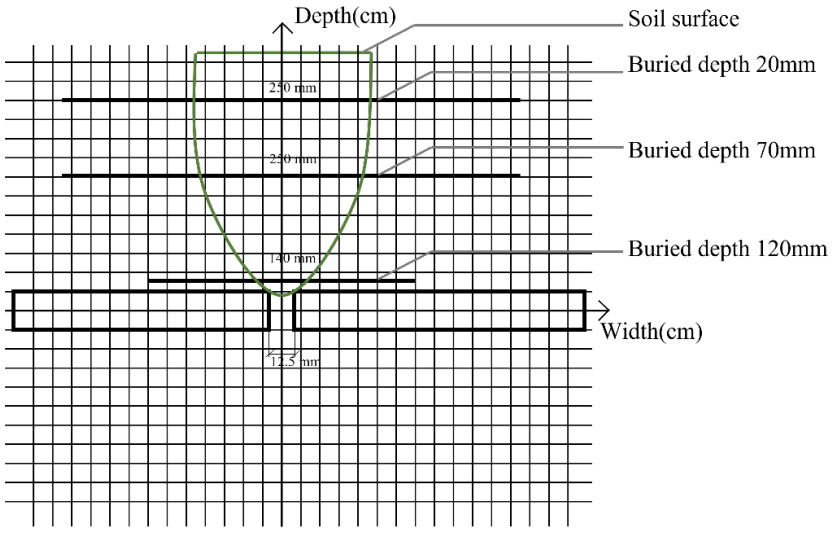

Figure 5. Reinforcement range diagram

2.3 Layout of Geogrid Position

Geogrid reinforcement is arranged near the top of the soil and in the middle of the soil. Under the condition of full pipe flow pressure and no reinforcement, the collapse area and loose area are relatively large, and there are erosion areas [29] (Figure 4, gray indicates the collapse area, yellow denotes the erosion area, and green represents stable regions). In order to reduce the loss of soil and slow down the erosion rate of water, the reinforced area should cross the collapse area and loose area, and keep a certain drawing area in the stable area to prevent the geogrid from being eroded by the eroded soil. The reinforcement range is shown in Figure 5. Geogrids are arranged in three positions to further explore the influence of geogrid reinforcement on the erosion process of subgrade soil. Due to

the wide erosion width of the upper soil, two geogrids with a width of 25 cm should be placed at the buried depths of 20 mm and 70 mm, respectively. The erosion area near the pipeline is small, so a small geogrid with a width of 14 cm should be placed at the buried depth of 120 mm above the pipeline fracture. In subgraph (b) of Figure 4 and Figure 5, grid spacing is 10 mm in both directions; Coordinate axes are in centimeters; labeled dimensions are in millimeters.

2.4 Experimental Scheme Design

The experiments were carried out under the condition of full pipe flow without geogrid and with geogrid, respectively. At room temperature between 26 and 30 °C, according to the volume ratio of 1:4, n-dodecane and 15# white oil were mixed to make a mixture. The mixed liquid is poured into the model box, and then the fused quartz sand is slowly dispersed into the mixed liquid and the glass rod or shovel is used to slowly stir the dispersed sand. After each dispersion into the sand, it is compacted and smoothed. The height of the mixed liquid is always 1∼2 cm higher than that of the sand, which can facilitate the separation of bubbles. When filling the pipeline position, the PVC pipe with an outer diameter of 25 mm is placed in advance at the reserved position in the box, and the whole PVC pipe with an outer diameter of 20 mm is placed in the pipe, and the fracture port size is set. At this time, the flanges on both sides need to be tightened with screws. After the sample preparation is completed, the shelf is fixed above the model box, and a laser transmitter and a camera are placed on the shelf to aim at the fracture port. The laser is turned on in advance during the test. A certain number of buckets are prepared on the left side of the model box to receive the test water. The right side of the model box is near the water source, and the water pipe is connected to the water source. The camera is placed below the front of the model box, and the SLR camera is placed in front of it (Figure 6). All cameras were turned on during the test, and the SLR camera was remotely controlled by a wireless device, and photographed every 2 s. During the test, the weight plates on the left and right sides need to be unloaded at the same time, and the internal pipeline is pulled out from the left side to simulate the sudden fracture state of the pipeline. When the water invasion test is carried out, the right side is connected to the water pipe first, and the left side has the water flow out, and then the pipe with an internal inner diameter of 20 mm is extracted. After the test, each surface of the erosion pit was photographed. The outflow sand and the mixture can be used twice after filtration. The sand mixed with water can be used twice after being dried in the sun.

In the process of sample preparation, the three geogrids were placed from low to high at the buried depth of 120 mm, the buried depth of 70 mm, and the buried depth of 20 mm, respectively, and the width of the fracture port was 12.5 mm. The full pipe flow condition simulates a pipeline filled with water or other liquids under high-pressure flow, such as during tap water transportation, urban flooding, or high-pressure gas and liquid transport in the petroleum and industrial sectors.

To ensure the reliability and repeatability of the findings, each experimental condition (with and without geogrid reinforcement) was independently repeated twice. The observations and quantitative measurements (including collapse depth and erosion area) were consistent across both trials, demonstrating good repeatability and experimental stability.

Figure 6. Model sample diagram

3 Results and Discussion

3.1 Soil Erosion Process

When the pipe flow is full without geogrids (flow rate is 0.5 L/s), the soil erosion process is shown in Figure 7, the water flow rushes into the soil at the beginning of the test, forming a cavity, and some water remains in the cavity. The erosion pit appeared at 18 seconds, and the pit became elliptical at 58 seconds. At 184 seconds, the erosion pit expands, the upper soil collapses to form a hole, and the soil flows out through the crack. At 218 seconds, the erosion pit was bowl-shaped, and the water and mixed liquid gradually flowed out. From 124 seconds, erosion occurred on the left side of the crack, and the erosion area was finally in the shape of a badminton [29].

In the case of full pipe flow with geogrid, the erosion process of soil caused by reinforced pipe fracture is shown in Figure 8, and the overall change is not obvious before 34 s. From 34 s to 60 s, the erosion pit gradually develops, and breaks through the first layer of geogrid at 60 s. At this time, the erosion pit is bowl-shaped, and the erosion pit gradually develops and becomes larger between 60 s and 176 s. At 198 s, the erosion pit broke through the second layer of geogrid. From 198 s to 436 s, the erosion pit was stable in a bowl shape. At 436 s after the test, the erosion pit did not change. No obvious erosion area was found in the whole test process at the fracture port. Due to the high water pressure when the pipe flow is full, water will continue to rush into the model from the fracture during the whole process of the test. The soil will collapse into the pipe under the combined action of gravity and seepage force, so that at the beginning of the test, there will be a hole at the upper surface corresponding to the fracture, and it will gradually develop and become larger with the test process.

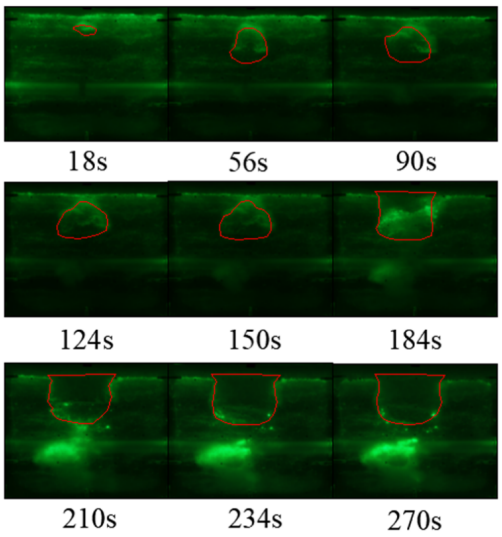

Figure 7. Full pipe flow unreinforced test process [29]

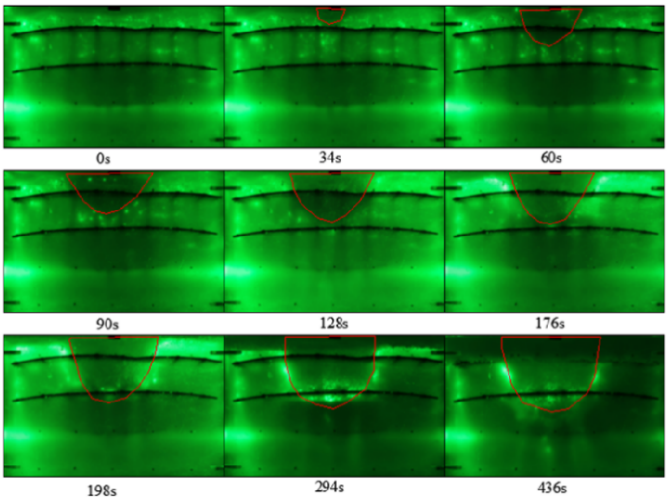

Figure 8. Full pipe flow reinforcement test process

3.2 Particle Motion Analysis

Using the difference method to analyze the image and perform pseudo-color output, the movement of the soil at different times can be obtained. In the figure, the blue area indicates that the particles are stationary, the red part indicates that the particle movement is the most intense, and the green part indicates that the particle movement intensity is between red and blue, grid spacing is 10 mm in both directions [29].

The particle motion observed under full pipe flow conditions without geogrid reinforcement is presented in Figure 9. At the beginning of the experiment, the pipeline was extracted to simulate a rupture, inducing a downward displacement of the overlying soil. An erosion pit began to form at approximately 18 seconds, during which intense particle movement was observed within the range of 80–130 mm on the Y-axis and –30–40 mm on the X-axis. Between 18 and 90 seconds, no visible surface deformation occurred; however, internal soil collapse progressed rapidly, accompanied by air ingress. During the intermediate phase of the test (90–150 seconds), the internal voids gradually expanded while particle activity diminished. At 185 seconds, the soil directly above the cavity suddenly collapsed into the fracture opening, resulting in renewed vigorous particle motion across the 0–130 mm range on the Y-axis and 70–80 mm on the X-axis, along with localized soil erosion. In the final stage of the experiment (184–234 seconds), the erosion pits became stably developed, water discharge was observed, and some regions remained structurally loose.

The particle movement under full pipe flow conditions with geogrid reinforcement is illustrated in Figure 10. At the initiation of the test (0 seconds), the internal pipeline was extracted to simulate a rupture, resulting in a downward displacement trend of the soil above the fracture zone. At approximately 34 seconds, intense particle movement was observed within the range of 60–130 mm on the Y-axis and –30–30 mm on the X-axis, accompanied by a pronounced downward trajectory that led to the formation of a loose soil zone. Surface-level erosion pits had already become visible at this stage. By 60 seconds, the erosion pit had progressed vertically to reach the first layer of geogrid reinforcement. During this phase, particle activity remained evident within the range of 80–110 mm on the Y-axis and –40–30 mm on the X-axis. Between 60 and 128 seconds, the erosion pit continued to develop between the first and second layers of geogrid, with the particle movement range extending from 80–120 mm on the Y-axis and –40–40 mm on the X-axis. From 128 to 294 seconds, the erosion pit further evolved, though the extent of particle motion gradually diminished, becoming concentrated around 70 mm on the Y-axis and remaining within –40–40 mm on the X-axis. By the end of the test at 436 seconds, the erosion pit had stabilized, with no further significant morphological changes observed.

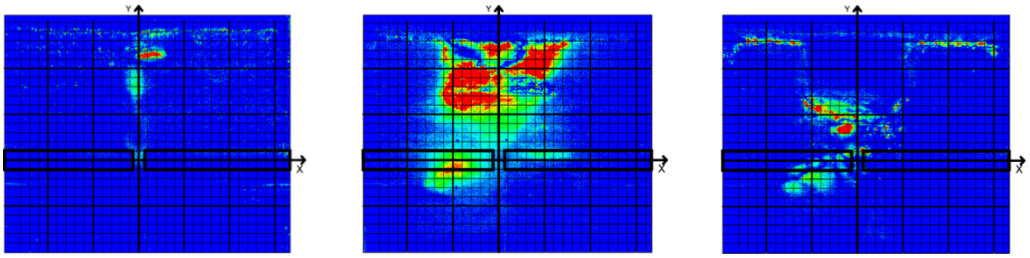

(a) The beginning of the experiment (t=18 s)

(b) Mid-term (t=184 s)

(c) The end of the experiment (t=234 s)

Figure 9. Motion of particles without geogrid [18]

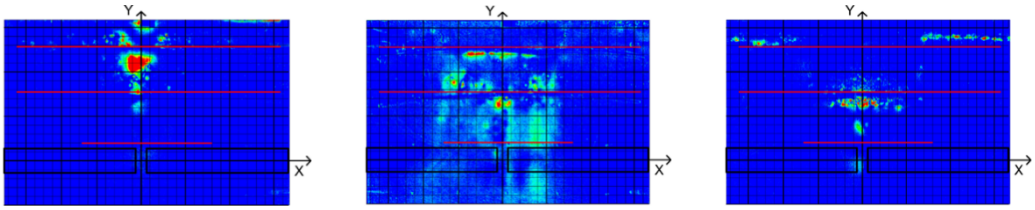

(a) The beginning of the experiment (t=34 s)

(b) Mid-term (t=128 s)

(c) The end of the experiment (t=294 s)

Figure 10. Motion of particles with geogrid

When no geogrid is added (subgraph (a) of Figure 11), the fast water flow under full pipe flow conditions carries away more soil, leading to the development of large erosion pits. In the process of erosion, secondary collapse will

occur, and voids will be formed inside the soil. The fast water flow speed will also obviously form the erosion area; when the geogrid is added (subgraph (b) of Figure 11), the interlocking and friction effects between the geogrid and the subgrade soil improve the overall stability of the subgrade, eliminate the sudden collapse inside the cavity, and significantly reduce the formation of erosion areas.

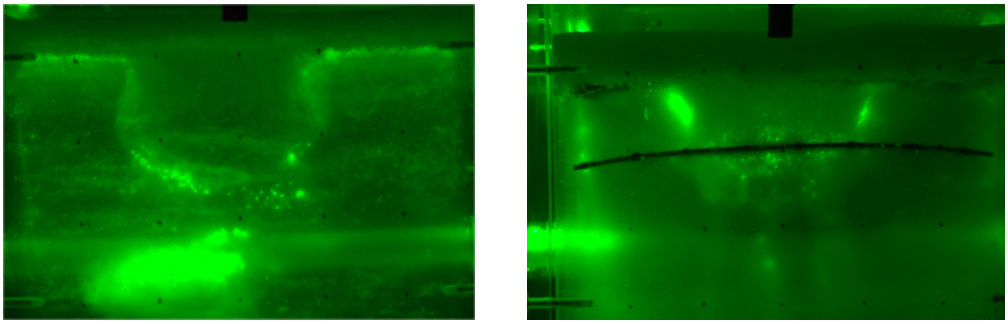

(a) Erosion pit without geogrid (b) Erosion pit with geogrid

Figure 11. Comparison of erosion pit

3.3 Comparative Analysis of Erosion Pit Size

By measuring the photos of the laser cross-section at each time period, the collapse depth and the area of the collapse area under different working conditions are obtained, as shown in Figure 12.

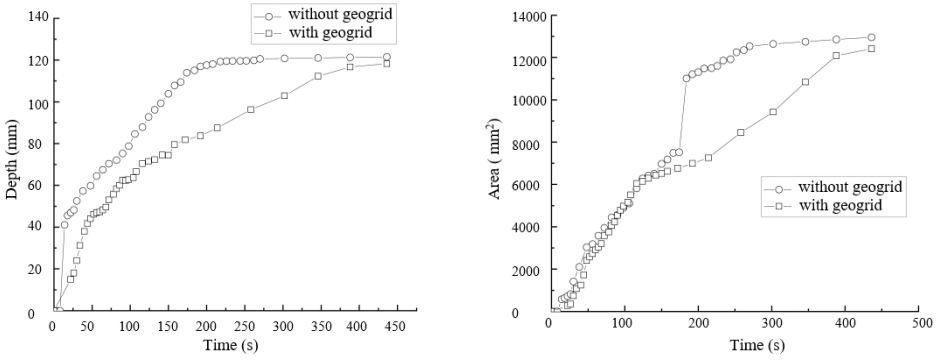

(a) Collapse depth (b) Collapse area

Figure 12. Erosion metrics comparison

From the perspective of collapse depth (as shown in subgraph (a) of Figure 12), in the case of no geogrid, the collapse suddenly occurred at 14 s, the collapse rate was faster before 174 s, and it slowly developed after 174 s until there was no collapse; in the case of geogrid, it suddenly collapsed at 22 s, the collapse rate was faster before 150 s, the collapse was slower than the front part from 150 s to 388 s, and the collapse slowed down from 388 s to 436 s until it was not collapsed. From 0s to 150s, the trend of the collapse depth of the erosion pit is roughly the same in the case of no geogrid and geogrid, but the depth of the geogrid is shallower than that of the no geogrid. From the 150 s onwards, the erosion pit depth curves of non-geogrid and geogrid began to show different trends. At about 200 s, the depth of the geogrid was 40 mm lower than that of the non-geogrid. When there is no geogrid, the depth of the erosion pit reaches 120 mm at 175 s. When there is geogrid, the depth of the erosion pit reaches 120 mm at 380 s, which is 205 s less than that without geogrid. When they reach the same depth, the time required in the case of geogrid is much longer than that without geogrid. In practical engineering, it can effectively slow down the erosion rate of pavement, thus providing buffer time for emergency repair.

From the cross-sectional area of the erosion pit (subgraph (b) of Figure 12), before 142 s, there was no significant change in the geogrid and non-geogrid under the full pipe flow state; however, at 174 s, the collapse suddenly occurred without geogrid, and the cross-sectional area of the erosion pit increased instantaneously. After 184 s, the collapse rate gradually slowed down, and the final cross-sectional area of the erosion pit was 12958 mm^2. In the case of geogrid, the existence of geogrid makes the overall collapse gentle, and there will be no sudden collapse phenomenon; after 142 s, the collapse rate became slower than before, and the final collapse area was 12415 mm^2.

When there is no geogrid, the erosion pit area reaches the peak at 180 s, and when there is geogrid, the erosion pit area reaches the peak at about 420 s, which is 240 s less than that without geogrid. When the two reach the same collapse area, the time required for the collapse of the erosion pit can be greatly reduced by adding the geogrid, which can effectively slow down the pavement erosion rate in the actual project, thus providing a buffer time for emergency repair.

3.4 Statistical Analysis of Collapse Data

To verify the significance of the observed differences between reinforced and unreinforced conditions, statistical analyses were performed on the measured collapse depth and cross-sectional area of the erosion pits.

3.4.1 One-way ANOVA

A one-way analysis of variance (ANOVA) was conducted to determine whether the use of geogrid reinforcement had a statistically significant effect on erosion pit depth and area.

Table 2. ANOVA results for the effect of geogrid on erosion depth and area

Variable	F-Value	p-Value	Significance
Depth	10.70	0.0016	Significant ($p < 0.01$)
Area	4.65	0.0344	Significant ($p < 0.05$)

Note: A significance threshold of 0.05 was used. Values of $p < 0.05$ indicate statistically significant differences between group

Table 2 presents the results of one-way ANOVA evaluating the effects of geogrid reinforcement on erosion depth and area. The analysis shows that the presence of geogrid has a statistically significant effect on erosion depth ($F = 10.70, p = 0.0016 < 0.01$), indicating a strong difference between the reinforced and unreinforced conditions. Similarly, for the erosion area, the effect is also significant ($F = 4.65, p = 0.0344 < 0.05$). These results confirm that geogrid reinforcement significantly mitigates both the extent and severity of soil collapse, supporting its effectiveness in improving subgrade stability.

3.4.2 Regression analysis

In order to quantitatively evaluate the influence of geogrid setting on local scour characteristics, based on the experimental data, the linear regression analysis was carried out on the change of scour depth and area with time in the two groups of 'with geogrid' and 'without geogrid', and the corresponding trend map was drawn as shown in Figure 13 and Figure 14.

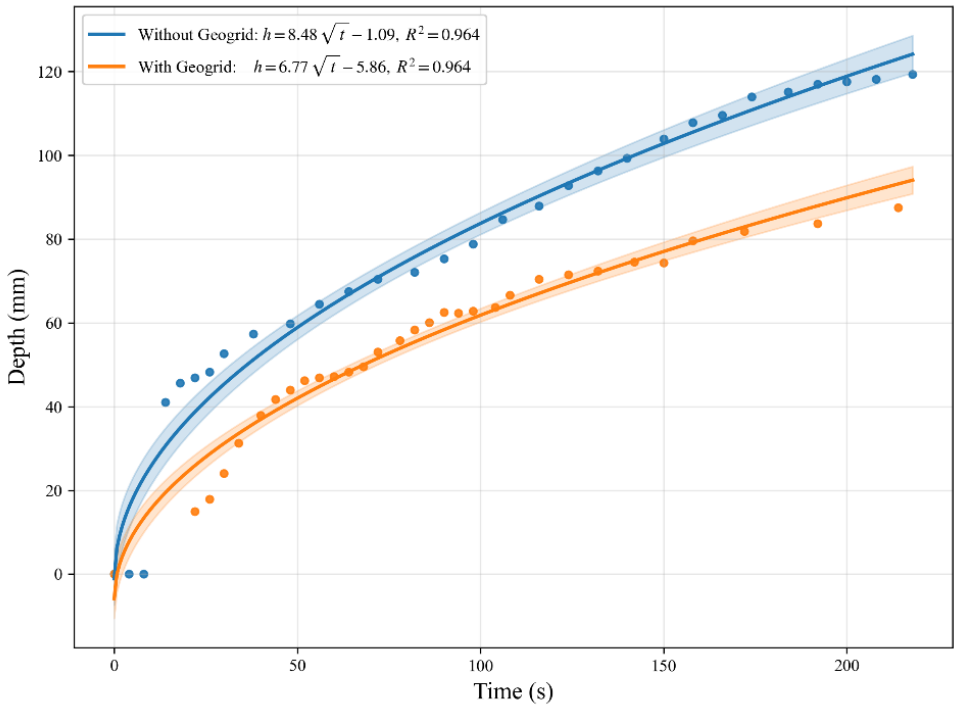

Figure 13. Regression of erosion depth over time

For scour depth (Figure 13), a square-root model was adopted:
(a) Without geogrid: $h = 8.48\sqrt{t} - 1.09, R^2 = 0.964$;
(b) With geogrid: $h = 6.77\sqrt{t} - 5.86, R^2 = 0.964$.
It can be observed that the growth rate of scour depth in the non-geogrid group is notably higher than that in the geogrid group. The coefficient of determination shows that both models have high goodness-of-fit, but the reduced slope in the geogrid case indicates an effective suppression of scour progression. One-way ANOVA further confirmed that there was a statistically significant difference in depth between the two groups ($F = 10.70, p = 0.0016 < 0.01$).

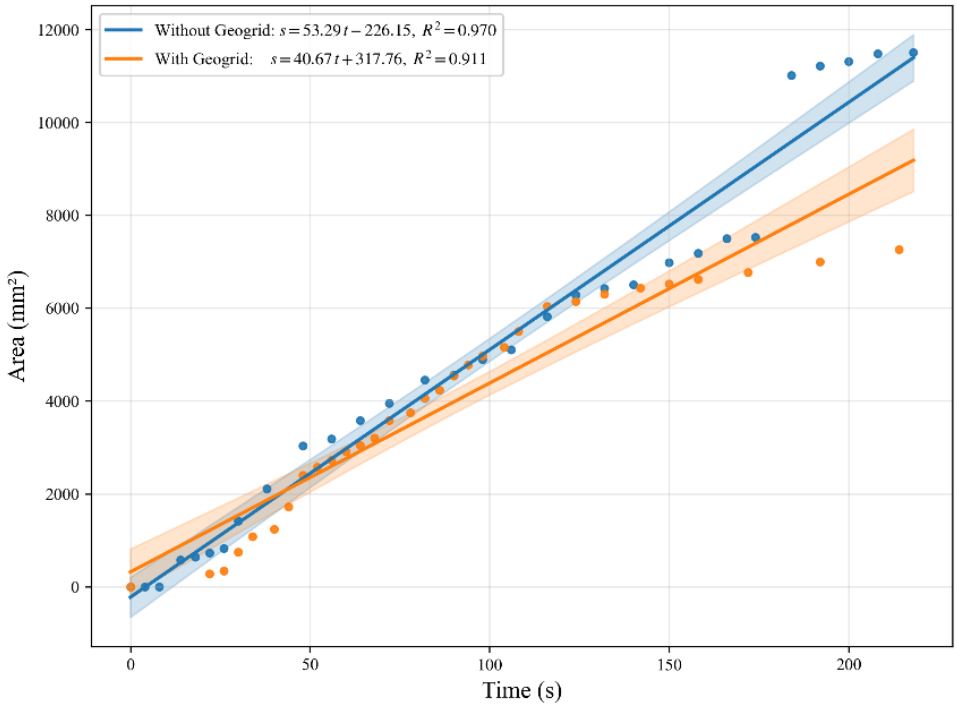

Figure 14. Regression of erosion area over time

For scour area (Figure 14), a linear model was applied:
(a) Without geogrid: $s = 53.29t - 226.15, R^2 = 0.970$;
(b) With geogrid: $s = 40.67t + 317.76, R^2 = 0.911$.
The slope for the unreinforced condition is markedly steeper, indicating a faster rate of area expansion, while the reinforced case exhibits a gentler slope, showing that geogrid not only reduces the overall erosion area but also slows the rate of progression. The interaction term between time and geogrid in the area regression model was statistically significant ($p = 0.001$), demonstrating that the effect of time on erosion area growth is dependent on the presence of geogrid reinforcement. This highlights geogrid's role in moderating erosion dynamics and providing more time for potential early intervention in practical applications.
In summary, the setting of geogrid shows a clear effect on controlling the depth and range of erosion, and has statistical significance and reliability, which effectively responds to the engineering objectives of the experimental design.
The geogrid reinforcement enhances soil stability through several synergistic mechanisms. Firstly, it increases frictional resistance and interlocking at the soil–geogrid interface, effectively constraining both horizontal and vertical displacement of soil particles. Secondly, the geogrid helps redistribute local stresses caused by soil collapse and hydraulic erosion, thereby preventing stress concentration and localized failure. Additionally, its tensile strength allows the geogrid to absorb and dissipate part of the kinetic energy from flowing water, reducing the erosive impact on the soil structure. Lastly, by confining the soil within defined spatial zones, the geogrid delays the development and propagation of internal voids and collapse fronts. Collectively, these mechanisms work to slow the initiation and evolution of collapse processes, resulting in a marked improvement in erosion resistance and overall subgrade stability.

4 Conclusions

Through the application of transparent soil modelling, the mechanisms of soil erosion and progressive collapse induced by pipeline rupture under full pipe flow conditions have been effectively visualized and analyzed. The

experimental findings confirm the significant role of geogrid reinforcement in enhancing the stability of subgrade soils and mitigating the extent and severity of collapse. In scenarios where no reinforcement was applied, large internal erosion zones were observed beneath the surface, progressing rapidly following pipe failure. By contrast, the inclusion of geogrid reinforcement considerably reduced the formation and propagation of these zones. This was attributed to the interlocking and frictional resistance between the geogrid and surrounding subgrade material, which served to constrain particle mobility, delay cavity expansion, and suppress sudden internal collapses. These effects contributed to a marked reduction in both the depth and area of the collapse zone. Specifically, the final measured collapse depth under full pipe flow with geogrid reinforcement was 108 mm—13 mm less than the unreinforced case—and the collapse area was 12,415 mm^2, representing a 543 mm^2 reduction compared to the 12,958 mm^2 observed without reinforcement. These quantitative reductions underscore the stabilizing effect of geogrid in subgrade environments subjected to hydraulic disturbance.

The experimental observations further indicate that the erosion pit developed more gradually in the reinforced condition, with its final geometry remaining smaller and structurally more stable than in the unreinforced scenario. Importantly, no sudden internal collapse was recorded in the presence of geogrid layers, suggesting that reinforcement not only enhances load-bearing resilience but also extends the time available for emergency intervention during pipeline failures. From a geotechnical engineering perspective, these findings provide a strong basis for improving subgrade reinforcement strategies, particularly in urban environments where pipelines are subjected to high-pressure flow conditions and aging infrastructure poses increasing risks.

Beyond the laboratory validation, the implications of this study extend to practical applications in infrastructure design and emergency management. The quantifiable relationship between collapse depth and affected area may serve as a foundational reference for threshold-based early warning systems in urban infrastructure, especially in high-risk zones prone to ground subsidence due to pipeline ruptures. In terms of reinforcement design, the results support the strategic placement of geogrid at critical depths (e.g., 20 mm, 70 mm, and 120 mm), offering practical guidelines for optimizing subgrade configurations in roadways, metro tunnels, and municipal pipeline systems. The observed ability of geogrid reinforcement to delay the onset of collapse and reduce erosion volumes translates into enhanced safety margins for real-world applications, facilitating longer lead times for monitoring, detection, and emergency response during pipe bursts or hydraulic incidents. Furthermore, this study validates the utility of transparent soil modelling as an effective visualization and simulation tool in underground construction and soil-structure interaction research, enabling more accurate and reproducible experimental analyses.

Despite the promising outcomes, certain limitations remain. The choice of geogrid material was limited to a single type, and alternative material types or configurations were not evaluated. Additionally, the positioning and spatial arrangement of reinforcement layers were fixed and not varied extensively. These constraints may influence the generalizability of the conclusions across a broader range of geotechnical scenarios. Future research should therefore consider a wider variety of geogrid materials, including those with differing tensile properties and mesh geometries. Coupling physical modelling with advanced numerical simulations is also recommended, as it would enable the parametric investigation of reinforcement layout, hydraulic loading regimes, and soil–structure interactions under controlled virtual environments. Such efforts are expected to enhance the generalizability and predictive accuracy of geogrid reinforcement strategies for mitigating collapse and erosion in pipeline-affected subgrades.

Data Availability

The data used to support the findings of this study are available from the corresponding author upon request.

Conflicts of Interest

The authors declare that they have no conflicts of interest.

References

[1] M. Bai, Y. Qi, L. Song, Q. Wang, Z. Zhang, and G. Tian, "Research on real-time monitoring and early warning of Tangshan road surface subsidence based on InSAR," *Adv. Space Res.*, vol. 75, no. 6, pp. 4408–4430, 2025. https://doi.org/10.1016/j.asr.2024.12.022

[2] H. Poorahong, P. Jamsawang, N. Thanasisathit, P. Jongpradist, and S. Horpibulsuk, "Enhancing the bearing capacity of unpaved roads on soft clay subgrade using geogrid reinforcement with a triaxial configuration," *Constr. Build. Mater.*, vol. 456, p. 139321, 2024. https://doi.org/10.1016/j.conbuildmat.2024.139321

[3] S. M. Tafreshi, H. A. Balf, H. R. Rezaeinejad, B. C. O'Kelly, and A. Faramarzi, "Bearing pressure enhancement of sand foundation beds by encapsulating geogrids in thin densified gravel layer inclusions," *Geom. Eng.*, vol. 40, no. 4, p. 277, 2025. https://doi.org/10.12989/gae.2025.40.4.277

[4] A. Erdağ, S. Fırat, M. Y. Fares, N. S. Işık, and B. Çetin, "Performance evaluation of geogrid-stabilized steel slag layer of pavement under repeated cyclic loading," *Transp. Geotech.*, vol. 53, p. 101603, 2025. https://doi.org/10.1016/j.trgeo.2025.101603

[5] M. S. Hussain, A. M. Shaban, and H. H. Hussein, "Geogrid reinforcement for improving bearing capacity and stability of square foundations," *Open Eng.*, vol. 14, no. 1, p. 20240021, 2024. https://doi.org/10.1515/eng-2024-0021

[6] X. Li, Y. Zhu, T. Su, X. Wang, and X. Zhang, "Study on performance improvement of new geocell reinforced asphalt mixture," *Constr. Build. Mater.*, vol. 273, p. 121693, 2021. https://doi.org/10.1016/j.conbuildmat.2020.121693

[7] A. Erdağ, B. Çetin, and S. Fırat, "Evaluation of resilient modulus and permanent deformation of steel slags and subgrade soil stabilized with geogrid material," *Constr. Build. Mater.*, vol. 471, p. 140640, 2025. https://doi.org/10.1016/j.conbuildmat.2025.140640

[8] W. Hassan, K. Farooq, H. Mujtaba, B. Alshameri, A. Shahzad, M. N. Nawaz, and M. Azab, "Experimental investigation of mechanical behavior of geosynthetics in different soil plasticity indexes," *Transp. Geotech.*, vol. 39, p. 100935, 2023. https://doi.org/10.1016/j.trgeo.2023.100935

[9] R. Zhang, Y. Zhou, Y. Guo, J. Zheng, Y. Deng, and T. Lan, "Influence of geogrid reinforcement on the cracking characteristics of expansive soils: A laboratory study," *Geotext. Geomembr.*, vol. 53, no. 2, pp. 545–558, 2025. https://doi.org/10.1016/j.geotexmem.2024.11.014

[10] M. C. Santos, C. Yoo, and F. H. M. Portelinha, "Influence of rainfall and drying periods on the performance of a large-scale segmental GRS wall model built with poorly draining local soil," *Geotext. Geomembr.*, vol. 53, no. 4, pp. 847–866, 2025. https://doi.org/10.1016/j.geotexmem.2025.02.003

[11] A. Elshesheny, M. Aljaberi, S. Almanea, and M. Mohamed, "Reducing load transfer to buried pipes through coupled use of geogrid reinforcement and sand rubber zone in the backfill material," *Transp. Infrastruct. Geotech.*, vol. 11, no. 6, pp. 3878–3902, 2024. https://doi.org/10.1007/s40515-024-00421-7

[12] D. Minchala, B. Gottumukkala, P. S. Prasad, and S. T. Swarna, "Performance evaluation of marginal materials in geosynthetic reinforced base layers," *Road Mater. Pavement Des.*, vol. 26, no. 3, pp. 706–719, 2025. https://doi.org/10.1080/14680629.2024.2373228

[13] X. Jiang, F. Zhang, B. Huang, H. Titi, P. Polaczyk, Y. Ma, and Z. Cheng, "Full-scale accelerated testing of geogrid-reinforced inverted pavements," *Geotext. Geomembr.*, vol. 52, no. 4, pp. 511–525, 2024. https://doi.org/10.1016/j.geotexmem.2024.01.005

[14] M. Saily and I. Gratchev, "Effect of geosynthetics on swell reduction during an extreme rainfall event," *Int. J. Geosynth. Ground Eng.*, vol. 9, no. 6, p. 78, 2023. https://doi.org/10.1007/s40891-023-00500-8

[15] M. R. Abdi, H. Mirzaeifar, Y. Asgardun, and K. Hatami, "Assessment of pegged geogrid (PG) pullout performance in coarse-grained soils using PIV analysis," *Geotext. Geomembr.*, vol. 52, no. 1, pp. 27–45, 2024. https://doi.org/10.1016/j.geotexmem.2023.09.001

[16] M. Iskander, R. J. Bathurst, and M. Omidvar, "Past, present, and future of transparent soils," *Geotech. Test. J.*, vol. 38, no. 5, pp. 557–573, 2015. https://doi.org/10.1520/GTJ20150079

[17] A. A. Ganiyu, A. S. A. Rashid, and M. H. Osman, "Utilisation of transparent synthetic soil surrogates in geotechnical physical models: A review," *J. Rock Mech. Geotech. Eng.*, vol. 8, no. 4, pp. 568–576, 2016. https://doi.org/10.1016/j.jrmge.2015.11.009

[18] M. G. Iskander, J. Lai, C. J. Oswald, and R. J. Mannheimer, "Development of a transparent material to model the geotechnical properties of soils," *Geotech. Test. J.*, vol. 17, no. 4, pp. 425–433, 1994. https://doi.org/10.1520/GTJ10303J

[19] M. Ahmed and M. Iskander, "Evaluation of tunnel face stability by transparent soil models," *Tunn. Undergr. Space Technol.*, vol. 27, no. 1, pp. 101–110, 2012. https://doi.org/10.1016/j.tust.2011.08.001

[20] G. Yu, Y. Cui, L. He, Y. Li, and H. Feng, "Influence of the soil-structure interface on seepage characteristics in uniformly-grained soils: Microscopical insights from transparent soil experiments," *Soils Found.*, vol. 65, no. 2, p. 101596, 2025. https://doi.org/10.1016/j.sandf.2025.101596

[21] N. Sanvitale, B. D. Zhao, E. T. Bowman, and C. O'Sullivan, "Particle-scale observation of seepage flow in granular soils using PIV and CFD," *Géotechnique*, vol. 73, no. 1, pp. 71–88, 2023. https://doi.org/10.1680/jgeot.20.P.432

[22] Z. Xu and Z. Guo, "Experimental study on bearing characteristics and soil deformation of necking pile with cap using transparent soils technology," *Adv. Civ. Eng.*, vol. 2021, no. 1, p. 6625556, 2021. https://doi.org/10.1155/2021/6625556

[23] X. Le, X. Cui, M. Zhang, Z. Xu, and L. Dou, "Behavior investigation of necking pile with caps assisted with transparent soil technology," *Sustainability*, vol. 14, no. 14, p. 8681, 2022. https://doi.org/10.3390/su14148681

[24] G. Siemens, C. Oldroyd, and R. Beddoe, "Flow cell with high-resolution spatial and temporal degree of saturation measurements for two-dimensional near-surface phenomena using unsaturated transparent soil," *Geotech. Test. J.*, vol. 44, no. 6, pp. 1713–1736, 2021. https://doi.org/10.1520/GTJ20200082

[25] L. Zhang, H. Liu, X. Ding, R. Chen, H. Zhou, Y. Li, and X. Ren, "Development of transparent soil grouting

test system and its application in grouted gravel pile," *Measurement*, vol. 234, p. 114899, 2024. https://doi.org/10.1016/j.measurement.2024.114899

[26] A. Ads, M. S. Islam, and M. Iskander, "Longitudinal settlements during tunneling in soft clay, using transparent soil models," *Tunn. Undergr. Space Technol.*, vol. 136, p. 105042, 2023. https://doi.org/10.1016/j.tust.2023.105042

[27] H. Liu, Z. Zong, W. Zhang, W. Sun, W. Ye, Z. Liu, and Q. Xu, "Impact of deep braced excavation on the deformation of existing tunnel by way of transparent soil model test," *Int. J. Phys. Model. Geotech.*, pp. 1–12, 2025. https://doi.org/10.1680/jphmg.24.00034

[28] B. Ok, M. Ünverdi, M. Seyedzavvar, C. Boğa, and T. Sarici, "3D-printed geogrids' tensile performance: Impact of filament type," *Rapid Prototyp. J.*, vol. 31, no. 7, pp. 1473–1488, 2025. https://doi.org/10.1108/RPJ-09-2024-0403

[29] Y. Duan, W. Zhang, H. Liu, and J. Chen, "Dynamics of soil erosion due to underground pipeline fractures: A transparent soil study under varied hydraulic conditions," *J. Comput. Methods Sci. Eng.*, vol. 24, no. 4–5, pp. 2429–2445, 2024. https://doi.org/10.3233/JCM-247466

[30] L. Jiang, B. Zhang, S. Huang, and Y. Shao, "Analysis of fluidized zone in transparent soil under jet induced by pipe leakage," *Water Sci. Eng.*, vol. 16, no. 2, pp. 203–210, 2023. https://doi.org/10.1016/j.wse.2023.01.002